summed Cu(I) van der Waals radii (2.8 Å) displayed the LE emission. Notably, Cu-Cu distances of those $Cu_4Cl_4L_4$ clusters for which crystal structures have been reported exceed 2.8 Å in each case;[42] e.g., the Cu-Cu distance for the nonemissive $Cu_4Cl_4(Et_3N)_4$ cluster is 3.07 Å.[30] This observation is consistent with the conclusion[20] that the LE emission band from the iodide $Cu_4I_4L_4$ clusters is a property of the Cu_4X_4 core and involves extensive interaction between the Cu(I) centers owing to the σ-bonding nature of the LUMO for those clusters with short metal-metal distances.

(42) Other examples of $Cu_4Cl_4L_4$ clusters which have been shown by X-ray crystallography to have the cubane type structure as in A with Cu-Cu distances in excess of 2.8 Å include those where L = 2-(diphenylmethyl)pyridine (2.901 Å),[32] 2-[bis(trimethylsilyl)methyl]pyridine (2.960 Å),[30] PPh_3 (3.306 Å),[33a] and PEt_3 (3.211 Å).[33b]

Acknowledgment. This research was supported by the U.S. National Science Foundation (Grant CHE 87-22561). We thank Professor G. Stucky for allowing access to the diffuse-reflectance spectrometer, Dr. V. Srdanov for helping with the DR measurements, and Dr. N. L. Keder for aid in X-ray powder diffraction studies.

Registry No. $Cu_4Cl_4(py)_4$, 104475-18-5; $Cu_4Cl_4(Phpy)_4$, 136144-92-8; $Cu_4Cl_4(DEN)_4$, 80105-82-4; $Cu_4Cl_4(mor)_4$, 136144-93-9; $Cu_4Cl_4(Et_3N)_4$, 97665-61-7.

Contribution from the Lehrstuhl für Theoretische Chemie, Technische Universität München, 8046 Garching, Federal Republic of Germany, Department of Physics and Astronomy, Northwestern University, Evanston, Illinois 60201, and Anorganisch-Chemisches Institut, Technische Universität München, 8046 Garching, Federal Republic of Germany

Electronic Structure of Main-Group-Element-Centered Octahedral Gold Clusters

A. Görling,† N. Rösch,*,† D. E. Ellis,‡ and H. Schmidbaur*,§

Received March 7, 1991

Molecular orbital calculations have been performed for the octahedral cluster ions $\{[(H_3P)Au]_6X_m\}^{m+}$ (X_1 = B, X_2 = C, X_3 = N) by using the first-principles self-consistent discrete-variational Xα method. The fragments Au_6^{2+} and $[(H_3P)Au]_6^{2+}$ have also been investigated, and the interpretation of their electronic structure forms the basis for an understanding of the main-group-element-centered clusters. Furthermore, a nearest-neighbor extended Hückel model is used to aid in elucidating the electronic structure of Au_6^{2+}. A major result, at variance with previous models for bonding in gold cluster compounds, is the prominent contribution of Au 5d orbitals, which is found to be as important as that of Au 6s orbitals. Their interplay, s-d hybridization, is symmetry-dependent and synergistic with both radial Au-ligand σ bonding and tangential Au-Au bonding. Relativistic effects strongly enhance this interaction mechanism and therefore are significant for the overall stability of the clusters. The central atom formally takes up four electrons that would otherwise reside in energetically unfavorable molecular orbitals, and it contributes to the stability of the cluster by forming radial bonds. Orbital and favorable electrostatic interactions decrease along the series X = B, C, N. However, for the boron-centered compound, repulsion between radially nonbonding Au d electron density and B 2p-derived density strongly reduces (or outweighs) the favorable interactions. The bonding interactions in the yet unsynthesized boron-centered cluster may be increased by employing more electronegative functional groups on the phosphine ligands although possibly at the expense of solvation and crystal packing problems. The flavor of the molecular orbital analysis, given here for octahedral gold clusters, notably the important role of Au 5d-6s hybridization, may be transferred to other gold cluster compounds, especially the closely related five-coordinated systems $\{[(R_3P)Au]_5Y_m\}^{m+}$ (Y_1 = C, Y_2 = N).

1. Introduction

The chemistry of gold has gained a new facet through the recent synthesis of the pentakis and hexakis auro methanium, ammonium, and phosphonium cations $\{[(C_6H_5)_3PAu]_5C\}^+$ (**1**), $\{[(C_6H_5)_3PAu]_5N\}^{2+}$ (**2**), $\{[(C_6H_5)_3PAu]_5P\}^{2+}$ (**3**), and $\{[(C_6H_5)_3PAu]_6C\}^{2+}$ (**5**).[1-4] Recent claims regarding the synthesis of $\{[(C_6H_5)_3PAu]_6N\}^{3+}$ (**6**) so far are unconfirmed.[5]

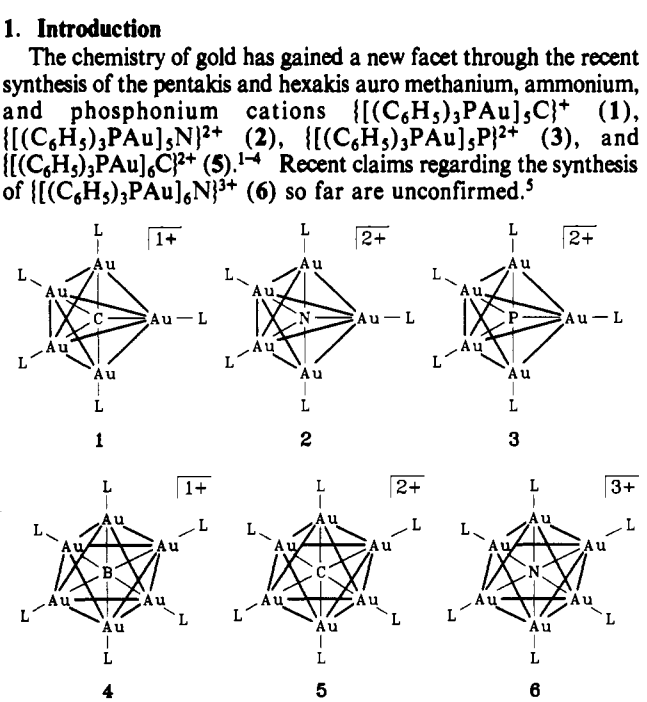

1 **2** **3**

4 **5** **6**

The existence of these astonishing compounds provides interesting challenges to electronic structure theory. The cations exhibit a highly symmetrical structure (the gold atoms forming a regular trigonal bipyramid or octahedron) and thus invite theoretical analysis. The second- or third-row main-group element at the center is five- or six-coordinate and therefore violates the classical octet rule. Furthermore, the cluster ions feature quite short distances between the gold atoms indicative of bonds between the d^{10} monovalent coinage metal atoms. The term "aurophilicity"[1] has been coined to denote the phenomenon that polyaurated organogold compounds seem to have a strong propensity to bind more gold(I) units, $[LAu]^+$ (L = R_3P), to a central atom. Particularly striking examples are the compounds cited above, but other less symmetrical compounds have been synthesized.[6,7] Since gold is the heaviest coinage metal and it forms these unusual cations, it seemed likely that relativistic effects play a role in this type of bonding. A preliminary analysis of the electronic structure

* Authors to whom correspondence should be addressed.
† Lehrstuhl für Theoretische Chemie, Technische Universität München.
‡ Northwestern University.
§ Anorganisch-Chemisches Institut, Technische Universität München.

(1) Scherbaum, F.; Grohmann, A.; Huber, B.; Krüger, C.; Schmidbaur, H. *Angew. Chem.* **1988**, *100*, 1602; *Angew. Chem., Int. Ed. Engl.* **1988**, *27*, 1544.
(2) Scherbaum, F.; Grohmann, A.; Müller, G.; Schmidbaur, H. *Angew. Chem.* **1989**, *101*, 464; *Angew. Chem., Int. Ed. Engl.* **1989**, *28*, 463.
(3) Grohmann, A.; Riede, J.; Schmidbaur, H. *Nature* **1990**, *345*, 140.
(4) Schmidbaur, H. *Gold Bull.* **1990**, *23*, 11.
(5) Brodbeck, A. Ph.D. Thesis, Universität Tübingen, 1990.
(6) Schmidbaur, H.; Graf, W.; Müller, G. *Angew. Chem.* **1988**, *100*, 439; *Angew. Chem., Int. Ed. Engl.* **1988**, *27*, 417; *Helv. Chim. Acta* **1986**, *69*, 1748.
(7) Schmidbaur, H.; Hartmann, C.; Reber, G.; Müller, G. *Angew. Chem.* **1987**, *99*, 1189; *Angew. Chem., Int. Ed. Engl.* **1987**, *26*, 1146.
(8) Pyykkö, P. *Chem. Rev.* **1988**, *88*, 563.

0020-1669/91/1330-3986$02.50/0

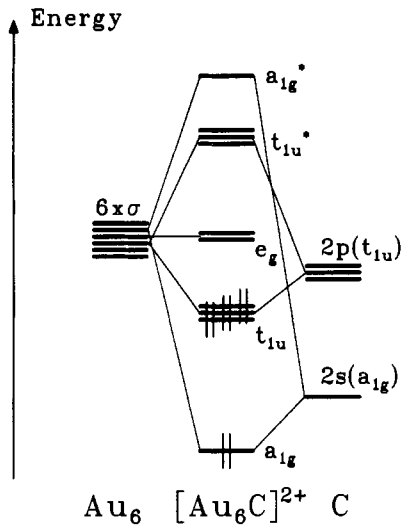

Figure 1. Schematic orbital interaction diagram for the carbon-centered cluster $[Au_6C]^{2+}$. Only Au orbitals pertinent to the bonding with the central carbon atom are shown. Formally the cluster Au_6^{2+} and the central atom each contribute four valence electrons.

of octahedral gold clusters has indeed confirmed the importance of relativistic effects for the bonding of these cluster compounds.[9] Correlation effects may have to be taken into account for a quantitative description of Au–Au bond distances if they are of similar importance as found in a recent study of multinuclear copper complexes.[10] Furthermore, a comparison of the electronic structure between the hexahydride cluster $(LCu)_6H_6$ and the carbon-centered cluster $[(LAu)_6C]^{2+}$ has recently been performed by using an approach similar to that used in the present study.[11]

Quantum chemical investigations of main-group-element-centered gold cluster compounds were started in the mid-1970s when the synthesis of an uncentered octahedral cluster cation $\{[(C_6H_5)_3PAu]_6\}^{2+}$ was reported.[12] It is nowadays assumed that this cluster actually contained an unrecognized carbon center.[1] Mingos studied hexaauro compounds using extended Hückel theory (EHT) and first discussed the possible existence of the centered cation **1**.[13] Arguments for the stability of this cluster ion and its diamagnetic nature are easily derived from a simple MO interaction diagram (see Figure 1). One caveat seems appropriate here. It will turn out that Figure 1 represents only a qualitative picture of the cluster bonding. Nevertheless, it may serve as a device for counting electrons and for pointing out the symmetry of the relevant molecular orbitals. The EHT investigations have been extended receently to larger gold cluster compounds.[14,15] An earlier self-consistent calculation, although restricted to the naked cluster Au_6^{2+}, was performed by using the Dirac scattered-wave–Xα (DSW-Xα) method.[16] In a relativistic pseudopotential Hartree–Fock (HF) calculation on Au_nX^{m+} (X = B – N, Al – S; n = 4–6), the variation of the equilibrium distance of the bond from the central atom to the surrounding gold atoms has been investigated.[17] The first all-electron study on the ligated carbon-centered octahedral gold cluster, performed by us using the same quantum chemical method as in the present study, provided evidence[9] that both a self-consistent relativistic treatment and the inclusion of the ligands are necessary for a satisfactory understanding of the underlying electronic structure problem. Previous theoretical investigations fall short in at least one of these essential features. EHT has well-known limitations as an electronic structure method, and for the systems under consideration previous results[13-15] will have to be supplemented even on a qualitative level as will be shown in this work. The HF study[17] suffers substantially from the fact that it does not treat the ligands; the DSW investigation[16] is restricted to the bare metal cluster.

With this work we continue a preliminary study[9] mentioned above, which was based on the discrete-variational–Xα (DV–Xα) method. It started with systems where the phosphine ligands are replaced by hydrogen sulfide, SH_2, for technical reasons.[9] Here a molecular orbital analysis of the octahedral cations **4–6** $\{[(H_3P)Au]_6X_m\}^{m+}$ (X_1 = B, X_2 = C, X_3 = N), and fragments thereof will be presented which we shall try to couch in such a form that allows a general interpretation of the electronic structure of this class of cluster compounds. Special emphasis will be placed on the influence of relativistic effects. Therefore, all calculations were performed in a nonrelativistic as well as a relativistic fashion. After addressing some computational details of the DV method, we first consider the fragment Au_6^{2+} and then turn to the cations $\{[(H_3P)Au]_6\}^{2+}$ and $\{[(C_6H_6)_3PAu]_6C\}^{2+}$. A discussion of octahedral clusters centered by nitrogen or boron will follow where special attention will be paid to the stability of the yet unsynthesized boron- and nitrogen-centered clusters.

2. Computational Details

The DV–Xα method is a self-consistent first-principles LCAO–MO procedure based on density functional theory that exists in a nonrelativistic and a relativistic version (for details see refs 18–20). In the relativisitic case, the molecular orbitals are built from four component Dirac spinors. The basis set consists of numerically generated atomic orbitals that are adjusted during the SCF process according to the atomic configurations determined in a Mulliken population analysis of the cluster. The DV–Xα method takes into account all electrons, but the core orbitals are kept fixed at their atomic shape, a very satisfactory approximation for the present purpose. Here the 1s orbitals of the central main-group-element atom X and the neon-like core of phosphorus are kept "frozen". For gold, the xenon-like core and the 4f shell are kept fixed, but the 5d, 6s and 6p orbitals are treated as valence orbitals. The core cutoff was taken at 1.0, 1.6, and 2.6 au for X, Au, and P, respectively. Matrix elements were obtained by numerical integration on a grid of about 24 000 points. The distribution of points at each atom was adjusted so that their numbers were in the ratio of approximately 0.55:1.0:0.36:0.12 for X, Au, P, and H, respectively. These sampling points were generated according to a Fermi distribution characterized by a width parameter of 1.0 and a radius of 2.0 au. The SCF procedure was halted when the atomic populations used to generate the basis set and those calculated for the cluster differed by less than 0.02 for each atomic subshell.

Octahedral symmetry was assumed for the cluster core Au_6X, and the full model cluster $\{[(H_3P)Au]_6X_m\}^{m+}$ was investigated in idealized D_{3d} symmetry. For the cluster $(LAu)_6X$, a standard geometry was abstracted from the experimental data[1] of $\{[(C_6H_5)_3PAu]_6C\}^{2+}$ and used in all further cluster calculations. It is characterized by the distances d(Au–X) = 212.5 pm, equivalent to a gold–gold distance of d(Au–Au) = 300.5 pm, and d(Au–P) = 227.2 pm. The phosphine ligands were modeled by PH_3 units with the following structure:[21] d(P–H) = 141.5 pm, and $\angle$(H–P–H) = 93.3°. The present investigation focuses on the molecular orbital structure; therefore, no geometry variation was considered. Using the same geometry for the other central atoms, boron and nitrogen, allows a clear discrimination of their influence without having to worry about possible geometrical effects. As judged from the known pentacoordinate carbon- and nitrogen-centered clusters, this appears to be a very good approximation, since these have essentially the same average Au–Au distances (300.8 pm).[5]

(9) Rösch, N.; Görling, A.; Ellis, D. E.; Schmidbaur, H. *Angew. Chem.* **1989**, *101*, 1410; *Angew. Chem., Int. Ed. Engl.* **1989**, *28*, 1357.
(10) (a) Schwerdtfeger, P.; Dolg, M.; Schwarz, W. H. E.; Bowmaker, G. A.; Boyd, P. D. W. *J. Chem. Phys.* **1989**, *91*, 1762. (b) Bauschlicher, C. W.; Langhoff, S. R.; Partridge, H. *J. Chem. Phys.* **1989**, *91*, 2412. (c) Kölmel, C.; Ahlrichs, R. *J. Phys. Chem.* **1990**, *94*, 5536. (d) Pyykkö, P.; Zhao, Y. *Angew. Chem.* **1991**, *103*, 622.
(11) Bowmaker, G. A.; Görling, A.; Rösch, N.; Schmidbaur, H. To be published.
(12) Bellon, P.; Manassero, M.; Sansoni, M. *J. Chem. Soc., Dalton Trans.* **1973**, 2423.
(13) Mingos, D. M. P. *J. Chem. Soc., Dalton Trans.* **1976**, 1163.
(14) Mingos, D. M. P. *Nature* **1990**, *345*, 113.
(15) Mingos, D. M. P.; Kanters, R. P. F. *J. Organomet. Chem.* **1990**, *384*, 405.
(16) Arratia-Perez, R.; Malli, L. *Chem. Phys. Lett.* **1986**, *125*, 143.
(17) Pyykkö, P.; Zhao, Y. *Chem. Phys. Lett.* **1991**, *177*, 103.
(18) Ellis, D. E.; Painter, G. S. *Phys. Rev. B* **1970**, *2*, 2887.
(19) Rosén, A.; Ellis, D. E. *J. Chem. Phys.* **1975**, *62*, 3039.
(20) Rosén, A.; Ellis, D. E.; Adachi, A.; Averill, F. W. *J. Chem. Phys.* **1976**, *65*, 3629.
(21) Weast, R. C. Ed. *Handbook of Chemistry and Physics*, 61th ed.; CRC Press: Boca Raton, FL, 1980.

Table I. Irreducible Representations Induced by Atomic Orbitals Located at the Vertices of an Octahedron[a]

orbitals	irreducible representations	orbitals	irreducible representations
s, p_z, d_{z^2}	a_{1g}, e_g, t_{1u}	$d_{x^2-y^2}$	a_{2g}, e_g, t_{2u}
(p_x, p_y), (d_{xz}, d_{yz})	t_{1u}, t_{2u}, t_{1g}, t_{2g}	d_{xy}	a_{2u}, e_u, t_{2g}

[a] The local z axis is directed toward the center of the octahedron.

Table II. Diatomic Overlap Integrals between 5d Orbitals of Neighboring Au Atoms in Au_6^{2+}

type	DVM[a]	EHT[b]
S_σ	0.039	0.026
S_π	0.025	0.011
S_δ	0.002	0.001

[a] Derived from nonrelativistic DVM results. For details see the Appendix. [b] Reference 12.

3. Results and Discussion

3.1. The Cluster Au_6^{2+}. The electronic structure of the Au_6^{2+} unit will serve as a first reference for our analysis. Formally, the electronic structure of each Au atom may be characterized by a d^{10} shell. Four electrons remain in cluster orbitals built mainly from Au 6s and 6p orbitals (see Figure 1). An interesting topic is the extent to which d orbitals contribute to the Au–Au bonding. In an LCAO–MO framework this can only be achieved if the closed-shell configuration of the d shell is broken, e.g. through s–d interaction.[8] In the following discussion, we will therefore examine the role of the 5d orbitals and their interaction with the 6s orbitals. The Au 6p orbitals will be treated together with the 6s orbitals since their importance for the bonding of the cluster is rather small. The p_z orbitals contribute slightly by polarizing s orbitals. The minor role of the 6p orbitals is a consequence of the fact that, especially in the relativistic treatment, hardly any s–p or p–d hybridization but mainly s–d hybridization is observed (see below).

Furthermore, we will use the cluster Au_6^{2+} to explain our notation and some essential group theory. To label the atomic orbitals of each gold atom we introduce a local coordinate system at each vertex of the octahedron, with the z axis directed toward the center of the cluster and with the x and y axes above the edges of the octahedron.[22] Linear combination of Au atomic orbitals leads to basis functions that belong to irreducible representations of the point group O_h as listed in Table I.

Here and in the following section we use, as much as possible, the language of extended Hückel theory when analyzing the electronic structure of the cluster although the underlying results come from a first-principles DVM–Xα calculation. This will allow for an intuitive interpretation as well as for an easy comparison with the results of previous EHT calculations.[12-14]

We start by considering the molecular orbitals derived from Au 5d atomic orbitals. Four MOs, a_{2u}, e_u, a_{2g}, and t_{1g}, are determined by symmetry (see Table I). The remaining d orbitals interact with other d orbitals (e_g, t_{1u}, t_{2g}, t_{2u}) and/or with s orbitals (a_{1g}, e_g, t_{1u}). If we exclude at first any s–d interaction and if we restrict d–d interactions to nearest neighbors only (the latter being a very good approximation), then the manifold of the Au 5d MOs is determined in extended Hückel theory by only four parameters, the atomic orbital energy $IE_{eff}(5d)$ and the overlap integrals S_σ, S_π, and S_δ (see Appendix). An effective EH Hamiltonian may be deduced from the DVM results by using the four molecular orbitals that are determined by symmetry alone (a_{2u}, e_u, a_{2g}, t_{1g}). In Table II we compare the resulting overlap parameters to values that were used in the EHT calculations of ref 12. For the energy parameter one obtains $IE_{eff}(5d) = -16.78$ eV.

In Figure 2, the complete extended Hückel retrocalculated 5d manifold is compared to the valence levels of Au_6^{2+} as obtained directly from nonrelativistic and relativistic DVM calculations.

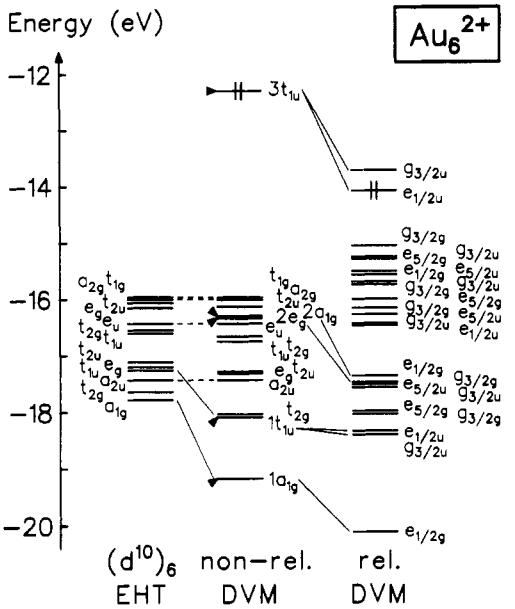

Figure 2. Comparison of nonrelativistic and relativisitic DVM–Xα results for the valence molecular orbital energies of Au_6^{2+}. Also shown is the EHT retrocalculated d manifold (see Appendix). The levels are labeled according to the irreducible representations of the groups O_h and O_h^*, respectively. The level occupation is indicated explicitly only for the HOMO of the cluster. Molecular orbitals important for s–d hybridization and Au–Au bonding are designated by wedges; lines connect related levels of the various model clusters.

Table III. Mulliken Population Analysis of Selected Molecular Orbitals with Au 6s and Au $5d_{z^2}$ Character and Total Valence Populations for the Cluster Au_6^{2+}

MO		energy, eV	Au s + p	Au d
$1a_{1g}$	nr[a]	−19.17	0.39	0.61
	rel[b]	−20.11	0.78	0.22
$1t_{1u}$	nr	−18.05	0.15	0.85
	rel	−18.38	0.27	0.73
$2e_g$	nr	−17.32	0.03	0.97
	rel	−17.47	0.03	0.97
$2a_{1g}$	nr	−16.34	0.63	0.37
	rel	−17.36	0.23	0.77
$3t_{1u}$	nr	−12.30	0.85	0.15
	rel	−13.84	0.63	0.37
tot.	nr		0.79	9.87
	rel		0.99	9.67

[a] Nonrelativistic calculation. [b] Relativistic calculation (spin–orbit average over corresponding molecular orbitals where appropriate).

The EH-derived spectrum and the nonrelativistic DVM spectrum are quite similar, except for a lowering of the orbitals $1a_{1g}$ and $1t_{1u}$ in the latter. This shows that simple MO arguments are sufficient to describe the main features of the electronic structure of Au_6^{2+}. The energetic lowering of the $1a_{1g}$ and $1t_{1u}$ MOs found in the DVM calculation is, of course, due to bonding Au 6s contributions, as is revealed by a Mulliken population analysis (see Table III).

The relatively large energy spacing of the d manifold in Au_6^{2+} is worth noting, about 1.8 eV for the retrocalculated EH spectrum and 3.2 eV for the DVM levels. This agrees quite well with the DSW results[15] but is at variance with previous EHT calculations.[12-14] Inspection of Table II reveals the reason for this major difference: all types of EHT overlap integrals between atomic d orbitals of neighboring gold atoms are smaller by about a factor of 2. This implies that the atomic orbitals used in the EHT calculation[12-14] do not have the proper extension or shape for modeling the interactions in the cluster Au_6^{2+} and would describe the Au 5d as totally localized and chemically inert. The shortcoming of the EHT spectrum is reminiscent of that found in previous comparisons between EHT, Xα, and experimental results for transition-metal clusters.[23,24]

(22) Messmer, R. P.; Knudson, S. K.; Johnson, K. H.; Diamond, J. B.; Yang, C. Y. *Phys. Rev. B* **1976**, *13*, 1396.

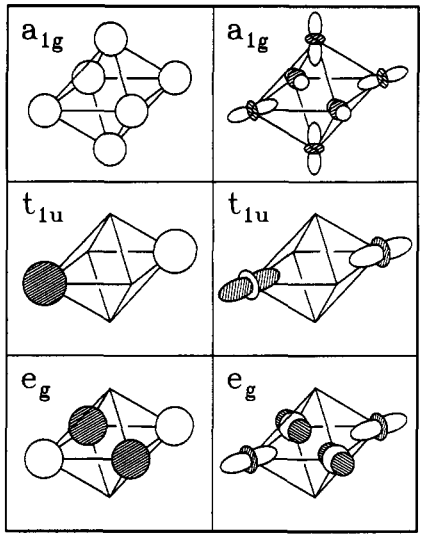

Figure 3. Sketches of bonding (a_{1g}), nonbonding (t_{1u}) and antibonding (e_g) linear combinations of Au 6s and $5d_{z^2}$ atomic basis functions important for s–d hybridization and the bonding of the cluster Au_6^{2+}. Only one linear combination is shown in cases of degeneracy.

The Au 6s orbitals lie at higher energy than the Au 5d orbitals and are more diffuse than the latter. However, these characteristics are not so different that Au 5d orbitals could be excluded from a discussion of the electronic structure, as in previous EHT-based treatments.[11-13] The DVM–Xα results show that a more complicated argument is necessary to account for the electronic structure of the system Au_6^{2+} and are a harbinger of what we will see for centered clusters, such as **5**.

The Au 6s orbitals in Au_6^{2+} belong to the irreducible representations a_{1g}, e_g and t_{1u} (see Figure 3), and s–d hybridization may, of course, occur only via 5d-derived MOs of like symmetry. Inspection of DV–Xα results show that to any significant degree only MOs generated from atomic orbitals of the d_{z^2} type (see Figure 2) are involved in this interaction. For the orbitals of symmetry e_g and t_{1u}, this statement implies some idealization, since 5d orbitals ($d_{x^2-y^2}$ or d_{xz}, d_{yz}; see Table I) are involved, but only to a very small degree. The s–d interaction between $5d_{z^2}$ and 6s orbitals leads to hybrid orbitals that are directed along the radial direction (the local z axis) or polarized parallel to the cluster surface (the local xy plane), respectively, with direct consequences for radial bonds to the central atom and to ligands. However, even in Au_6^{2+} some energy gain goes along with this hybridization, as can be seen from the difference between the retrocalculated EHT and the DVM–Xα orbitals of the $1a_{1g}$ and $1t_{1u}$ orbitals (see Figure 2).

It is easy to rationalize why s–d hybridization is strongest in orbitals of a_{1g} symmetry and weaker in those of e_g symmetry. The a_{1g} orbitals of s and of d_{z^2} type are both bonding. The s-derived MOs decrease more in energy than the d_{z^2}-derived MOs since the s orbitals overlap more strongly. Thereby the s–d energy difference in the a_{1g} manifold is reduced compared to the corresponding atomic energies, facilitating their interaction. Indeed, the Au 6s orbital of a_{1g} symmetry ($2a_{1g}$ in Figure 2) is lowered far enough so that it lies within the 5d manifold, while the antibonding orbitals of e_g symmetry get pushed further apart as compared to the corresponding atomic energies. Therefore hybridization plays no role and the Au s level of e_g symmetry lies high in energy and is empty. The orbitals of type t_{1u} are nonbonding or slightly antibonding. The Au 6s orbital $3t_{1u}$ represents the HOMO of Au_6^{2+}, occupied by two electrons (see Figure 2).

The MO spectrum obtained from a relativistic calculation of Au_6^{2+} is also shown in Figure 2. In the relativistic case the energy levels are labeled according to the irreducible representations of the double group O_h^*. Correlations may be constructed by using the rules $a_1 \rightarrow e_{1/2}$, $a_2 \rightarrow e_{5/2}$, $e \rightarrow g_{3/2}$, $t_1 \rightarrow e_{1/2} + g_{3/2}$, and $t_2 \rightarrow e_{5/2} + g_{3/2}$ (both for gerade and ungerade representations). In the relativistic case, there are more levels due to lower degeneracies and fewer irreducible representations, thus allowing for more interactions. A further complication is introduced by spin–orbit splitting, which is taken into account implicitly. The orbitals of interest ($1a_{1g}$, $2a_{1g}$, $2e_g$, $1t_{1u}$, $3t_{1u}$) essentially keep their character and can be easily identified (see Figure 2). This is also true for larger systems, like $\{[(H_3P)Au]_6C\}^{2+}$. For the sake of simplicity, we shall therefore keep the familiar nonrelativistic symmetry labels also in the relativistic case. Any numerical results for the t_{1u} orbitals will be given as a weighted average over the corresponding $e_{1/2u}$ and $g_{3/2u}$ orbitals.

It is well-known that a relativistic electronic structure treatment of gold leads to a contraction of the 6s shell with a concomitant lowering in energy whereas the 5d shell becomes more diffuse and rises in energy.[8] This implies that the differences, both in energy and in spatial character, between these two types of valence orbitals decrease, increasing the possibility of an even stronger s–d interaction. This expectation is confirmed by the even larger energy splitting of the relativistic DVM–Xα level spectrum (see Figure 2; one further notes a separation of the d manifold into two parts due to spin–orbit interaction). The lowering of the Au 6s orbitals is reflected in the corresponding decrease of the $2a_{1g}$ and the $3t_{1u}$ orbitals. Inspection of Table III reveals a stronger s–d mixing in the orbitals of type a_{1g} and t_{1u}. In the case of the a_{1g} orbitals, it is so strong that it hardly makes sense any more to speak of s- and d-derived orbitals. This larger hybridization together with the lowering of the Au 6s orbital energy is responsible for the decrease in energy of the $1a_{1g}$ and $1t_{1u}$ orbitals.

To summarize we note that the electronic structure of Au_6^{2+} is characterized by distinctive d–d and s–s interactions, as well as by a strong s-d hybridization. The view of a largely inert 5d shell is not appropriate, especially if relativity is taken into account, which strengthens all these interactions.[9] However, the interpretation of the electronic structure obtained on the basis of nonrelativistic results remains qualitatively valid in the relativistic case. We would like to mention that the type of s–d hybridization invoked here has also been used in the discussion of linear two-coordinate Au(I) compounds.[24]

3.2. The Cluster $[(H_3P)Au]_6^{2+}$. With the PH_3 ligands added to the Au_6 fragment, the symmetry of the system is reduced from O_h to D_{3d} and the O_h levels of type t are split into a + e. Under D_{3d}, the MOs of pertinent interest, a_{1g}, e_g, and t_{1u}, are labeled a_{1g}, e_g, and $a_{2u} + e_u$, respectively. However, in the core part of the cluster (including the P–Au σ bonds) the original octahedral symmetry is essentially maintained since all splittings are small. We leave aside the H–P bonds, which are of no interest in the present context. It is practical to label all energy levels with the symbols of the group O_h and to average values over split levels as they occur. The phosphine lone-pair orbitals subduce MOs of symmetry a_{1g}, e_g, and t_{1u} in $[(H_3P)Au]_6^{2+}$, which will interact with the corresponding orbitals of Au_6^{2+}. Their energy is comparable to that of the $1t_{1u}$ orbital of Au_6^{2+}.

In the spirit of the analysis of the previous section, we formally count three relevant valence orbitals, Au s and d_{z^2} and $\sigma(PH_3)$, and four electrons per $(H_3P)Au$ unit: the remaining four electrons are later attributed to the central carbon in the cluster $\{[(H_3P)Au]_6C\}^{2+}$.

If we start with symmetry a_{1g} and assume in a first formal step that the Au 5d orbitals form a pair of bonding and antibonding MOs with the ligand orbitals (see Figure 4a), the Au 6s orbital, nonbonding under this assumption, should lie energetically between these orbitals. When mixed into the other two MOs, this orbital acquires some Au 5d character (see Figure 4b). Lowest in energy is a H_3P–Au bonding orbital whose gold fraction is an s–d hybrid that points in the Au–P bond direction. Next in energy is a pure

(23) Rösch, N.; Knappe, P.; Sandl, P.; Görling, A.; Dunlap, B. I. In *The Challenge of d and f electrons. Theory and Computation*; Salahub, D. R., Zerner, M. C., Eds.; ACS Symposium Series 394; American Chemical Society: Washington, DC, 1989; p 180.

(24) (a) Bancroft, G. M.; Chan, T.; Puddephatt, R. J.; Tse, J. S. *Inorg. Chem.* **1982**, *21*, 2946. (b) Chastain, S. K.; Mason, R. W. *Inorg. Chem.* **1982**, *21*, 3717.

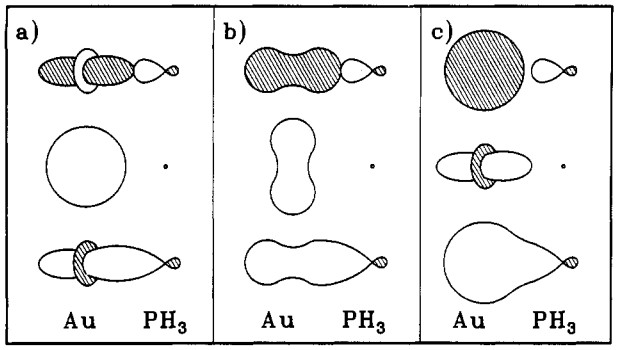

Figure 4. Sketches illustrating various interaction schemes of the orbitals important for the bonding in the cluster $[LAu]_6^{2+}$: Au $5d_{z^2}$, Au 6s, and σ(L). Only the situation at one vertex is shown. Key: (a) Au–L bonding and antibonding linear combinations of Au(d) and σ(L), Au(s) Au–L nonbonding; (b) s–d hybridization favoring Au–L radial bonding as well as Au–Au tangential bonding; (c) Au–L bonding and antibonding linear combinations of Au(s) and σ(L), Au(d) Au–L nonbonding.

Table IV. Mulliken Population Analysis of Selected Molecular Orbitals with Au 6s and Au $5d_{z^2}$ Character and Total Valence Populations for the Cluster $[Au(PH_3)]_6^{2+}$

MO		energy, eV	Au s + p	Au d	PH_3
$1a_{1g}$	nr[a]	−16.65	0.17	0.57	0.26
	rel[b]	−16.36	0.39	0.29	0.32
$1t_{1u}$	nr	−15.82	0.04	0.51	0.45
	rel	−15.48	0.08	0.25	0.67
$1e_g$	nr	−15.42	0.02	0.46	0.53
	rel	−15.17	0.06	0.27	0.67
$2a_{1g}$	nr	−13.14	0.76	0.24	0.00
	rel	−13.53	0.42	0.50	0.08
$3a_{1g}$	nr	−12.47	0.32[c]	0.10	0.59
	rel	−12.43	0.23[c]	0.36	0.42
$3t_{1u}$	nr	−12.04	0.28	0.38	0.34
	rel	−11.29	0.12	0.80	0.08
$3e_g$	nr	−11.50	0.18	0.46	0.36
	rel	−10.78	0.16	0.73	0.12
$4t_{1u}$	nr	−8.63	0.69[c]	0.08	0.23
	rel	−8.80	0.50[c]	0.19	0.31
tot.	nr		1.04	9.77	7.86
	rel		1.29	9.59	7.79

[a] Nonrelativistic calculation. [b] Relativistic calculation (spin–orbit average over corresponding molecular orbitals where appropriate). [c] Here, the Au 6p contribution dominates over the Au 6s contribution (see text).

Au s–d orbital that is hybridized along the cluster surface and is H_3P–Au nonbonding. These two orbitals are filled. There remains the empty H_3P–Au antibonding orbital whose gold fraction is again an s–d hybrid. All three orbitals are Au–Au bonding due to their overall totally symmetric form.

The same conclusions may be reached if we start with the molecular orbitals of Au_6^{2+} given in the previous section. There, two Au s–d hybridized orbitals are obtained, the first one directed along the local z axis, the other parallel to the cluster surface. The former can easily interact with the ligand lone-pair orbitals, building the H_3P–Au bonding and antibonding orbitals, while the latter exhibits only little interaction with the ligands and remains roughly phosphine–Au nonbonding.

The situation described so far is supported by our DVM–Xα results. In Table IV, the Mulliken populations of relevant orbitals of $[(H_3P)Au]_6^{2+}$ are collected. The orbitals $1a_{1g}$ and $2a_{1g}$ indeed show s–d mixing, which, in the relativistic case, gives results of about equal weight. Furthermore, only a small H_3P contribution is found in the $2a_{1g}$ orbital. The foregoing analysis is corroborated by the overlap populations listed in Table V, which demonstrate the bonding and nonbonding nature of the orbitals $1a_{1g}$ and $2a_{1g}$, respectively. In $[(H_3P)Au]_6^{2+}$, the orbital $3a_{1g}$ is also occupied and carries electrons that later will be formally donated to the yet missing central atom. This MO has a positive P–Au overlap population, at variance with the above analysis (see Table V).

Table V. Au–P Overlap Populations for Selected Orbitals of $[Au(PH_3)]_6^{2+}$, Comparing Nonrelativistic and Relativistic Results

MO	nr	rel	MO	nr	rel
$1a_{1g}$	0.12	0.16	$3a_{1g}$	0.13	0.07
$1t_{1u}$	0.13	0.14	$3t_{1u}$	0.10	0.04
$1e_g$	0.17	0.19	$3e_g$	0.06	0.03
$2a_{1g}$	−0.01	−0.02	$4t_{1u}$	0.00	−0.04

Together with the orbital $4t_{1u}$, it provides the only exception (among all systems studied here) where Au 6p contributions play a role as can be seen in a more detailed population analysis not displayed here. In this way the four extra electrons help to stabilize the hypothetical cluster $[(H_3P)Au]_6^{2+}$. However, this special situation will not continue once a central atom has been introduced into the octahedron, and we can then restrict our analysis again to Au s and d orbitals.

Our analysis started from the idealized situation of Au d orbitals interacting with ligand lone pair orbitals, the Au s orbitals not yet being involved, and then considered the effect of Au s–d mixing. This resulted in a replacement of some Au d character in the various MOs by Au s contributions and vice versa. If this trend continued, one would end up with a situation where the H_3P–Au orbitals would exhibit only Au s character and the third, nonbonding orbital would be of pure Au d type (see Figure 4c). This is the interaction scheme corresponding to inert Au 5d shells, a situation not supported by our DVM–Xα results, but sometimes used to interpret the electronic structure of gold compounds and, at least to some extent, modeled by EHT calculations.[13,15]

Now, we briefly consider the remaining relevant orbitals of symmetries e_g and t_{1u}. For e_g symmetry, we start again with H_3P–Au(5d) bonding and antibonding orbital pairs, but the unperturbed Au 6s MO now lies above the antibonding phosphine–Au MO due to the strongly Au–Au antibonding nature of the e_g(Au s) orbital. The large energy separation prevents any effective s–d hybridization in the bonding H_3P–Au orbital. In its antibonding partner, some Au 6s contributions will help to diminish (or neutralize) the antibonding H_3P–Au(5d) interaction and introduce some H_3P–Au(6s) bonding character. The $1e_g$ level, as obtained in the DVM–Xα calculation, exhibits only little Au 6s character whereas the $3e_g$ orbital contains a noticeable Au s contribution (see Table IV). The corresponding overlap populations reveal the reasonably strong bonding P–Au character of the $1e_g$ orbital whereas the $3e_g$ orbitals are weakly P–Au bonding (see Table V). The last point implies that the bonding influence of the Au s contribution overcompensates for the antibonding influence of the Au d contribution (despite the fact that the second is larger) because the s orbital is somewhat more diffuse and therefore better suited for interaction with the ligands. It is worth noting that, in the relativistic case, the PH_3 contribution to the $1e_g$ orbital increases and that of the $3e_g$ orbital decreases (see Table IV). This is a consequence of the fact that the Au d orbitals rise in energy in a relativistic description.

The situation in t_{1u} symmetry is similar to the one just discussed for the e_g orbitals. However, the unperturbed Au s level is Au–Au nonbonding or only weakly antibonding. The energy difference to the Au d and ligand orbitals is therefore smaller than for e_g MOs, and s–d mixing is somewhat stronger.

After the preceding detailed molecular orbital analysis, we now would like to take a more general view of the electronic structure of the cluster $[(H_3P)Au]_6^{2+}$ that particularly emphasizes Au–Au interactions. If the Au 6s and 5d contributions were equally distributed over all relevant occupied orbitals of symmetries a_{1g}, e_g, and t_{1u}, then no contribution to Au–Au bonding would result since bonding and antibonding contributions would cancel. In a molecular orbital picture, to obtain a net Au–Au attraction, orbitals of Au–Au bonding character should feature a high Au s contribution because the Au s overlap is larger than the Au d overlap. In orbitals of Au–Au antibonding character the opposite situation would be favorable. How do the DVM–Xα results support such considerations? If one averages the populations of the two lowest-lying relevant levels in each symmetry, one obtains the following Au s and Au d contributions in the relativistic case:

Table VI. Mulliken Population Analysis of Selected Molecular Orbitals with Au 6s and Au $5d_{z^2}$ Character and Total Valence Populations for the Cluster $\{[(H_3P)Au]_6C\}^{2+}$

MO		energy, eV	C s	C p	Au s + p	Au d	PH_3
$1a_{1g}$	nr[a]	−20.13	0.70		0.05	0.21	0.05
	rel[b]	−19.54	0.65		0.12	0.17	0.05
$1t_{1u}$	nr	−16.06		0.19	0.02	0.47	0.33
	rel	−16.53		0.29	0.03	0.25	0.43
$1e_g$	nr	−15.25			0.02	0.37	0.61
	rel	−15.57	0.00		0.02	0.17	0.80
$2a_{1g}$	nr	−14.41	0.11		0.05	0.16	0.69
	rel	−14.65	0.11		0.08	0.06	0.75
$3a_{1g}$	nr	−12.45	0.00		0.50	0.40	0.10
	rel	−13.07	−0.01		0.33	0.65	0.03
$3t_{1u}$	nr	−11.96		0.03	0.22	0.43	0.32
	rel	−12.07		0.07	0.23	0.59	0.10
$3e_g$	nr	−11.10			0.17	0.57	0.26
	rel	−10.67	0.00		0.16	0.76	0.08
$4t_{1u}$	nr	−9.76		0.36	0.30	0.21	0.13
	rel	−10.22		0.30	0.12	0.39	0.19
tot.	nr		1.67	4.44	0.77	9.57	7.97
	rel		1.55	4.96	0.99	9.31	7.95

[a] Nonrelativistic calculation. [b] Relativistic calculation (spin–orbit average over corresponding molecular orbitals where appropriate).

a_{1g}, 0.40, 0.39; e_g, 0.11, 0.50; t_{1u}, 0.10, 0.53. The Au s population in the Au–Au bonding orbitals of a_{1g} symmetry is clearly higher than that in the orbitals belonging to e_g and t_{1u} symmetry. To appreciate this result, one should keep in mind that an average contribution of 0.40 in the two a_{1g} orbitals formally corresponds to a total population of 1.60 electrons.

We summarize at this point by noting that the DVM–Xα results for the cation $[(H_3P)Au]_6^{2+}$ support a distinctive Au–Au bonding interaction as a consequence of symmetry-dependent Au s–d hybridization. The phosphine–Au bonding is also affected by this s–d interaction.[13] One may interpret the above analysis in the way that the attempt to strengthen the Au ligand bond initiates Au s–d hybridization, with resulting Au–Au bonding. In any case, there is a peculiar interplay between the phosphine–Au and the Au–Au bonding. This may also be one of the reasons why in the HF calculation[17] where no ligands are present, essentially no Au–Au interaction was found. EHT results[15] yield only very weak Au–Au bonds because the s–d hybridization is not properly described in a nonrelativistic calculation.[9]

3.3. The Cluster $\{[(H_3P)Au]_6C\}^{2+}$. We shall base the discussion of the electronic structure of the carbon-centered cluster $\{[(H_3P)Au]_6C\}^{2+}$ (**5**) on that of the system $[(H_3P)Au]_6^{2+}$ as given above. The carbon atom at the center of the octahedron provides two new types of orbitals, its 2s and 2p orbitals belonging to the symmetry a_{1g} and t_{1u}, respectively. The C 2s orbital lies energetically below the MOs of $[(H_3P)Au]_6^{2+}$ and is filled. Its major contribution is to the $1a_{1g}$ orbital of **5** (see Table VI) with a small admixture of the $1a_{1g}$ orbital of $[(H_3P)Au]_6^{2+}$. The C 2p level is able to take up four more electrons, formally the four from the highest-lying orbitals of $[(H_3P)Au]_6^{2+}$, $3a_{1g}$ and $4t_{1u}$. One learns from a Mulliken population analysis of $\{[(H_3P)Au]_6C\}^{2+}$ that the C 2p orbitals contribute to the $1t_{1u}$ orbital and, even slightly more, to the cluster HOMO $4t_{1u}$ (see Table VI). This is at variance with the EHT results,[13] which find all orbitals with carbon contribution energetically below the Au d- and s-derived levels. The phosphine levels are also found below this manifold. Both observations may have a common cause: the lack of self-consistent consideration of the positive charge of the gold cluster.

Besides the Mulliken population analysis in Table VI we will make use of the overlap populations given in Table VII. We continue with a discussion of the a_{1g} orbitals. The orbital $2a_{1g}$ essentially corresponds to the H_3P–Au bonding orbital $1a_{1g}$ of $[(H_3P)Au]_6^{2+}$ with some antibonding C s contribution. The Au character is diminished compared to the latter orbital in favor of more PH_3 character. This is due to the antibonding admixture of C s and to the fact that the d orbitals of **5** lie higher altogether (see below). Orbital $3a_{1g}$ has nonbonding characteristics with respect to C–Au and H_3P–Au and corresponds to the $2a_{1g}$ orbital of $\{[(H_3P)Au]_6C\}^{2+}$. The $1a_{1g}$ orbital has a strong, positive C–Au overlap indicative of a corresponding bond, the $2a_{1g}$ orbital exhibits bonding H_3P–Au and antibonding C–Au overlap, as discussed above, and the $3a_{1g}$ orbital exhibits only small overlap populations in accordance with its nonbonding character. The depopulation of the high-lying $3a_{1g}$ orbital of $[(H_3P)Au]_6^{2+}$ stabilizes the cluster **5**.

Table VII. Au–P and Au–C Overlap Populations for Selected Orbitals of $\{[(H_3P)Au]_6C\}^{2+}$, Comparing Nonrelativistic and Relativistic Results

	Au–P		Au–C	
MO	nr	rel	nr	rel
$1a_{1g}$	0.00	0.01	0.24	0.29
$1t_{1u}$	0.13	0.17	0.11	0.03
$1e_g$	0.18	0.11		0.00
$2a_{1g}$	0.14	0.18	−0.03	−0.04
$3a_{1g}$	0.06	0.01	−0.01	−0.04
$3t_{1u}$	0.06	0.03	−0.09	−0.09
$3e_g$	0.05	0.04		0.00
$4t_{1u}$	−0.01	0.04	0.08	−0.12

The presence of the central atom does not seriously affect the character of the e_g orbitals as can be seen from Tables VI and VII. The $1e_g$ orbital remains Au–PH_3 bonding and has scarcely any Au s contribution whereas the $3e_g$ orbitals, as in $[(H_3P)Au]_6^{2+}$, can be classified as H_3P–Au(d) antibonding and H_3P–Au(s) bonding. The general raising of the Au d orbitals leads to an increased PH_3 contribution in the $1e_g$ orbital compared to $[(H_3P)Au]_6^{2+}$, whereas it is decreased in the $3e_g$ orbital.

As in $[(H_3P)Au]_6^{2+}$, the $1t_{1u}$ orbital is of H_3P–Au(d) bonding nature and contains hardly any Au s contributions, but it does exhibit an additional C 2p bonding admixture (see Table VII). However, in this context we should mention that the Mulliken populations and overlap populations of the t_{1u} orbitals, as obtained from the relativistic DV–Xα calculation, are of only limited interpretative value (see below). The $3t_{1u}$ orbital may be characterized as H_3P–Au(d) antibonding and H_3P–Au(s) bonding with some C 2p contributions. Being the counterpart of the $1t_{1u}$ orbital, the HOMO $4t_{1u}$ orbital contains significant C 2p character and an antibonding admixture of the H_3P–Au bonding orbital of $[(H_3P)Au]_6^{2+}$. This relatively high-lying level promotes s–d hybridization, which shows up in a C–Au bonding Au s contribution. Unfortunately, our results do not allow a unique classification of the C–Au bonding nature of this orbital since nonrelativisitic and relativistic overlap populations have different signs. This may to some extent arise from problems associated with the relativistic Mulliken population analysis (see below).

The general statements on the electronic structure of $[(H_3P)Au]_6^{2+}$, especially the discussion of s–d hybridization, also apply to $\{[(H_3P)Au]_6C\}^{2+}$. In the relativistic case, the Au s contributions to the a_{1g} molecular orbitals are about twice as large as those to the e_g MOs, the contributions to the t_{1u} MOs lying in between. As in $[(H_3P)Au]_6^{2+}$, one can correlate symmetry-dependent Au s–d hybridization with Au–Au bonding.

The presence of the central atom has two important consequences. First, there are direct orbital interactions between C and Au orbitals that overall are of bonding character for a_{1g} symmetry. In t_{1u} symmetry, our results in the nonrelativistic and relativistic case are not conclusive. The nonrelativistic results, as a whole indicating bonding interaction, are probably more reliable because of technical problems in connection with relativistic Mulliken populations in t_{1u} symmetry (see below). The second effect of the central atom is a formal charge transfer of four electrons out of high-lying orbitals in $[(H_3P)Au]_6^{2+}$ into the 2p orbitals of the central atom. Taken together, both orbital interactions via radial C–Au bonds and repopulation lead to a distinct gain in stability.

3.4. Comparison of Au_6 Systems with Different Central Atoms. The effect of different central atoms, X_1 = B, X_2 = C, and X_3 = N, on the charge distribution in the cluster $\{[(H_3P)Au]_6X_m\}^{m+}$, **4**–**6**, is displayed in Table VIII. We will first discuss the nonrelativistic results.

Table VIII. Comparison of Nonrelativistic and Relativistic Results for the Atomic Charges in $\{[(H_3P)Au]_6X_m\}^{m+}$ (X_1 = B, X_2 = C, X_3 = N)

central atom		X	Au	PH_3
B	nr[a]	−1.98	0.592	−0.093
	rel[b]	−4.92	1.120	−0.133
C	nr	−1.86	0.630	0.015
	rel	−2.80	0.832	−0.030
N	nr	−1.50	0.608	0.142
	rel	−1.31	0.570	0.147

[a] Nonrelativistic calculation. [b] Relativistic calculation.

In this case, the charge density assigned to the central atom increases with increasing nuclear charge in agreement with chemical expectation. The increase in charge from boron to nitrogen, about 1.5 electrons, is somewhat smaller than the corresponding change of the nuclear charge. Therefore, the negative charge of the central atom becomes smaller when going from boron to nitrogen. For the nonrelativistic calculations, the atomic charge of the Au_6 skeleton is almost independent of the central atom (see below). But the charge of the phosphine ligands becomes more positive when going from boron to nitrogen, as expected by chemical intuition. These findings correlate with the energy shift of those Au d levels that are not involved in the H_3P–Au or C–Au bonding. This manifold extends over the following energy range: N, −17.7 to −16.0 eV (relativistically −17.4 to −14.7 eV); C, −14.0 to −12.0 eV (relativistically −13.6 to −10.9 eV); B, −10.4 to −8.5 eV (relativistically −10.0 to −7.2 eV).

The energy of the radially nonbonding d orbitals depends, to first order, on the charge of the Au atoms, which is quite constant with X_m in the nonrelativistic calculation. To second order, this energy is influenced by surrounding charges. In the nitrogen-centered cluster, the Au atoms are surrounded by positively charged ligands and enclose the central atom, which carries the least negative charge in the series. Therefore, one easily rationalizes the low energy of the d orbitals. In the boron-centered system, on the other hand, with its negatively charged ligands and the relatively high negative charge on the central atom, the d manifold is highest in energy. In the reference system $[(H_3P)Au]_6^{2+}$, the d levels are found from −14.7 to −12.7 eV (relativistically −14.0 to −11.1 eV). This is lower than in the boron- and carbon-centered clusters, but higher than in the nitrogen-centered cluster. From the energy shift one concludes therefore that the additional electron density placed at the center of the cluster $[(H_3P)Au]_6^{2+}$ dominates the additional nuclear charge in the case of boron and carbon; for nitrogen, it is the other way around.

So far, orbital interactions have been stressed when the electronic structure of the clusters have been analyzed. We now consider electrostatic interactions as well. To this end we divide a cluster into three shells. The electron density within the Au_6 cage is assigned to the central atom. It dominates the corresponding nuclear charge and therefore constitutes a negatively charged region. Next comes the shell of the positively charged gold atoms. Between these two parts of the cluster, an electrostatic attraction occurs that stabilizes the whole system. The charge of the outer shell of ligands varies with the nature of the central atom and therefore shows a varying electrostatic interaction. According to this simplifying argument, the boron-centererd cluster gains the highest stabilization from electrostatic interaction because in this case the negative charge in the center region is largest and the Au–ligand interaction is attractive. The opposite situation holds in the nitrogen-centered cluster where the negative central charge is comparatively small and the Au–ligand interaction is repulsive.

Taking the H_3P–Au overlap population as a criterion, we note that the radial Au–ligand bonds remain almost unaffected during a change of the central atom, both in the nonrelativistic and in the relativistic calculations. Over all orbitals, we find a total population of about 4.0 electrons (relativistically 4.6). The X-Au bonding in the a_{1g} symmetry weakens in the series B, C, N as shown by the summed overlap population which decreases from 0.70 to 0.22 electron (relativistically from 0.60 to 0.22 electron). This may be rationalized as follows. With increasing nuclear charge the X 2s orbital shifts to lower energy and becomes more contracted, thereby leading to a reduction of the overlap with Au orbitals. In t_{1u} symmetry the X–Au overlap population decreases from 0.75 to 0.44 electron, again resulting in a weakening of the bond in the series B, C, N. In this case, the rationalization is a bit more involved. The 2p orbital of the central atom, the HOMO of the cluster, has a lower energy for X = N than for X = C. Therefore, the N–Au bonding interaction with the $1t_{1u}$ H_3P–Au orbital is strengthened compared to the C–Au bonding, whereas the interaction with the unoccupied high-lying Au s orbital (which is of X–Au bonding nature, too) decreases. The second effect dominates. Furthermore, the X–Au overlap becomes small since the nitrogen orbitals are more contracted. For boron, all trends compared to carbon are in the opposite direction. The foregoing arguments, concerning both the orbital as well as the electrostatic interaction, imply that the stability of the cations decreases in the series B, C, N.

Finally, we address the discrepancy in the atomic charges, both in size and in the trend over the series **4** to **6**, between nonrelativistic and relativistic calculations (see Table VIII). The relativistically determined Mulliken population of the central atom decreases from boron to nitrogen (from 7.92 to 6.31)—in contrast to the nonrelativistic results (from 4.98 to 6.50) and to chemical intuition. Connected with this odd behavior of the populations is the charge of the central atom, which decreases in the series B, C, N from −1.31 to the unrealistic value of −4.92. The formal charge of the Au atoms ranges from +0.57 to +1.12 in the series **4** to **6**. Detailed inspection of the results reveals that the puzzling behavior is caused almost exclusively by orbitals of t_{1u} symmetry (see above).

It is well-known that Mulliken populations obtained from a large LCAO basis set with diffuse functions may run against chemical intuition. The reason for this breakdown of the Mulliken procedure[25] is intimately connected with the fact that it does not necessarily provide the intended real space partitioning of the molecular charge. Diffuse basis functions centered on one atom may serve to describe the wave function and, ultimately, electron density in the vicinity of a second atom. It will be erroneously attributed to the first atom where it is centered. In the present variant of the DV method,[18-20] a minimal basis of optimally chosen numerical basis functions is used, and therefore, the described weakness should not cause any problems.

In the case of a boron-centered cluster (and to some extent also for its carbon analogue) where the central atom is closely surrounded by gold atoms, the following scenario may take place. The basis set is determined self-consistently with respect to populations attributed to each atomic subshell.[18-20] During the SCF process, the p orbitals of the negatively charged central atom become relatively diffuse and therefore acquire the capability of modeling charge density that chemical intuition would attribute to the surrounding gold atoms. In this way the B 2p population increases and, in turn, leads to even more diffuse B 2p basis functions when the basis set update takes place. Although the description of the molecular orbitals is highly accurate, the corresponding B 2p populations are useless for a chemical interpretation. The situation becomes noticeable only in the relativistic calculation because in this case the Au d orbitals are more diffuse and so their tails may be more easily replaced by B 2p functions when one is building the t_{1u} molecular orbitals.

Thus far the breakdown of the Mulliken population analysis has been presented as a more technical problem that prevents a satisfactory interpretation of the results. But it implies that B 2p functions are used to model Au d contributions and have thus become sufficiently diffuse. As a result, any occurring orbital interaction would be strengthened. But there is considerable Au d electron density in orbitals that do not interact with the central atom for symmetry reasons, and the corresponding electrostatic repulsion will increase. Put in somewhat oversimplified terms,

(25) Szabo, A.; Ostlund, N. S. *Modern Quantum Chemistry*; McGraw-Hill: New York, 1982.

Table IX. Overlap $\langle \chi_1^A | \chi_2^B \rangle$ between Atomic d Orbitals at Neighboring Vertices of an Octahedron Built Up from Two-Center Contributions of Type σ, π, and δ with a Common Factor $^1/_{16}$ Suppressed for Convenience, e.g $S_5 = (3S_\sigma + 4S_\pi + 9S_\delta)/16$

	atomic orbitals		local diatomic overlap		
overlap	site A	site B	σ	π	δ
S_1	z^2	z^2	1	12	3
S_2[a]	xz	yz	12		4
S_3[a]	xz	yz		8	8
S_4	xy	xy		8	8
S_5	$x^2 - y^2$	$x^2 - y^2$	3	4	9
S_6	xz	z^2	$2(3^{1/2})$		$-2(3^{1/2})$
S_7	yz	xy		8	−8
S_8	xz	$x^2 - y^2$	6		−6
S_9	z^2	$x^2 - y^2$	$-3^{1/2}$	$4(3^{1/2})$	$-3(3^{1/2})$

[a] There are two types of overlap between an xz orbital at one site and an yz orbital at a neighboring site. One, S_2, is dominated by σ interaction (e.g. sites 1 and 2 in the coordinate system of ref 28), the other, S_3, by π interaction (e.g. sites 1 and 3 in the coordinate system of ref 28).

the cage of gold atoms is not wide enough to hold a negatively charged central atom and therefore a repulsion with the B–Au nonbonding part of the Au d shell occurs. In our investigation, the cluster geometry was fixed according to the one of the carbon-centered system. The described repulsion could be reduced by increasing the B–Au bond length. But this would entail a larger Au–Au distance, too, weakening the Au–Au bonds.

In summary, the following conclusion may be drawn from our comparative study with different central atoms. Orbital interactions as well as electrostatic interactions lead to increasing stability of the cluster $\{[(H_3P)Au]_6X_m\}^{m+}$ in the series N, C, B. But in the case of boron, this stabilization is overcompensated for by a repulsion between the B 2p orbitals and the B–Au nonbonding Au d orbital contributions. Alternatively, a loss of Au–Au bonding would result if a lengthening of the B–Au bond is allowed. The present findings are consistent with HF results for the equilibrium bond distances of the clusters $[Au_6X_m]^{m+}$, where X_1 = B, X_2 = C, and X_3 = N.[17] There, the minimal bond length X–Au was found for the carbon-centered cluster and the longest for the boron-centered cluster. One should keep in mind, however, that our studies have shown that there is an intricate connection between the radial and the tangential bonds in the Au_6 backbone whereby the phosphine ligands increase the overall stability of the cluster ion. Therefore, results for the "naked" cluster $[Au_6X_m]^{m+}$ are only of limited relevance.

It is interesting to speculate whether the unfavorable interactions described above may explain why the cluster $\{[(R_3P)Au]_6B\}^+$ has not yet been synthesized and how their influence might be reduced. A possible alternative might call for a modification or a replacement of the commonly used triphenylphosphine ligands $P(C_6H_5)_3$. The charge of the Au atoms is quite independent of the central atom (at least in the nonrelativistic calculations), implying a charge exchange between the ligands and the central atom. Therefore by the use of more electronegative ligands, e.g. with halogen-substituted phenyl groups, charge might be "pulled" from the center of the cage to the ligand region. Of course, the electronic structure analyzed here is only one aspect that has to be considered in this context. Kinetic aspects, especially possible fragmentation steps of the cluster as well as the solvation effects or crystal packing effects, may be of importance. In connection with the latter two aspects, it is worth noting that the phosphine ligands of the cation synthesized so far (**5**, X = C) are calculated as neutral or positively charged. In the boron-centered cluster **4**, on the other hand, the phosphine ligands carry a negative charge (see Table VIII).

4. Conclusions

The present molecular orbital analysis of the clusters $\{[(H_3P)Au]_6B\}^+$, $\{[(H_3P)Au]_6C\}^{2+}$, and $\{[(H_3P)Au]_6N\}^{3+}$ and their fragments Au_6^{2+} and $[(H_3P)Au_6]^{2+}$ is based on first-principles self-consistent DVM–Xα calculations. A major result of this study

Table X. Energy Levels of the d Orbitals for an Octahedral Transition Metal Cluster According to the Nearest-Neighbor Extended Hückel Model for Overlap Values S_1–S_9 Collected in Table IX

sym	atomic orbitals	energy[a]
a_{1g}	z^2	$(1 + 4\kappa S_1)/(1 + 4S_1)$
t_{1g}	(xz, yz)	$(1 - 2\kappa S_2)/(1 - 2S_2)$
a_{2u}	xy	$(1 + 4\kappa S_4)/(1 + 4S_4)$
e_u	xy	$(1 - 2\kappa S_4)/(1 - 2S_4)$
a_{2g}	$x^2 - y^2$	$(1 - 4\kappa S_5)/(1 - 4S_5)$
t_{1u}	$(xz, yz), z^2$	$[1 + (\kappa + 1)S_3 - 8\kappa S_6^2 \pm (\kappa - 1)(S_3^2 + 8S_6^2)^{1/2}]/(1 + 2S_3 - 8S_6^2)$
t_{2g}	$(xz, yz), xy$	$[1 + (\kappa + 1)S_2 - 8\kappa S_7^2 \pm (\kappa - 1)(S_2^2 + 8S_7^2)^{1/2}]/(1 + 2S_2 - 8S_7^2)$
t_{2u}	$(xz, yz), x^2 - y^2$	$[1 - (\kappa + 1)S_2 - 8\kappa S_8^2 \pm (\kappa - 1)(S_3^2 + 8S_8^2)^{1/2}]/(1 - 2S_3 - 8S_8^2)$
e_g	$z^2, x^2 - y^2$	$[1 + (\kappa + 1)(S_5 - S_1) - 4\kappa S_1 S_5 - 12S_9^2 \pm (\kappa - 1)((S_1 + S_5)^2 + 12S_9^2)^{1/2}]/[(1 - 2S_1)(1 + 2S_5) - 12S_9^2)]$

[a] To be scaled with the d orbital ionization energy. κ denotes the Wolfsberg–Helmholtz constant, its customary value being 1.75.

is the prominent contribution of the Au 5d orbitals to the cluster bonding, at variance with a widely held view.[13-15] Their role in determining the stability of the cluster is as important as that of the Au 6s orbitals. Symmetry-dependent s–d hybridization leads to Au–Au bonding contributions and a strengthening of the Au–ligand bonds. The ligands support (or even initiate) Au s–d hybridization,[13] which strengthens all pertinent bonds, Au–Au and Au–ligand as well as Au–X (X = B, C, N). Therefore investigations of "naked" Au_6 clusters should underestimate the stability of the compounds. The present calculations show that s–d interaction is favored when relativistic effects are taken into account due to the resulting reduction of the energy difference and the increasing radial overlap of the Au s and d orbitals. Therefore, relativistic effects contribute significantly to the stability of the cluster compounds[9] and might reduce the impact of correlation effects,[10,17] which are difficult to ascertain separately in a local density-based approach, such as the present Xα calculation.[26]

The central atom formally takes up four electrons that otherwise would reside in energetically unfavorable molecular orbitals. Furthermore, it stabilizes the cluster by forming radial bonds to the shell of Au atoms. Electrostatic interactions between the negatively charged central atom and the positively charged Au_6 shell should also be taken into account. Orbital and electrostatic interactions lead to increasing cluster stability in the series of central atoms N, C, B. However, for the boron-centered compound, repulsion between electron density connected with the central atom and the Au d contributions leads to a strong destabilization that might outweigh the other favorable interactions. The present results, especially the symmetry dependence of the Au s–d hybridization and the resulting favorable Au–Au interaction, are of general validity and not restricted to systems containing six gold atoms, as shown by a study in progress on analogous Au_5 clusters. In summary, for a complete description of the electronic structure of main-group-element-centered gold clusters all interactions, Au–Au, Au–X, and Au–ligand, have to be taken into account.

Acknowledgment. This work was supported by the Deutsche Forschungsgemeinschaft (N.R.) and the Leibniz-Programm der Deutschen Forschungsgemeinschaft (H.S.), the Bund der Freunde der Technischen Universität München (N.R.), and the Fonds der Chemischen Industrie (N.R. and H.S.). It was initiated during a visit of D.E.E. to the Technische Universität München, which was supported in part through Sonderforschungsbereich 128 of the DFG.

(26) Sabin, J. R.; Trickey, S. B. In *Local Density Approximations in Chemistry and Solid State Physics*; Dahl, J. P., Avery, J., Eds.; Plenum: New York, 1984; p 333.

Appendix: Energy Levels for the d Electrons of an Octahedral Cluster

It is quite instructive for the interpretation of all-electron results to compute the d-electron energy levels of an octahedral complex analytically within the extended Hückel framework. One starts by introducing local coordinate systems at each vertex of the octahedron with the z axis directed toward the center of the cluster,[27,28] a very convenient choice. Due to the very localized nature of the involved atomic orbitals it is a very good approximation to neglect overlap between next-nearest neighbors, i.e. atoms at diagonally opposite vertices. In a first step, one expresses the overlap between d orbitals at neighboring sites in two-center contributions of type σ, π, and δ (see Table IX). Then symmetry-adapted linear combinations of atomic orbitals are formed for the various irreducible representations (see Table I). In Table X, the resulting energy levels are listed as functions of the overlap parameters S_1-S_9 in units of the effective atomic ionization energy IE_{eff}(Au 5d).

Using the nonrelativistic DVM level spectrum for the cluster Au_6^{2+}, one may deduce the four parameters of the model, S_σ, S_π, S_δ, and IE_{eff}(Au 5d) from levels a_{2g}, a_{2u}, e_u, and t_{1g}, which would not be affected if Au 6s orbitals were included in the EH model. The resulting overlap values are displayed in Table II. The corresponding full EH d level spectrum for Au_6^{2+} is shown in Figure 2.

Explicit EH-type calculations on octahedral transition metal clusters have been performed previously.[27,28] In ref 28, some corrections to the expressions published of ref 27 have been given. However, the formulas of ref 28 are incomplete in so far as they neglect interactions between orbitals of the same irreducible representation, but of different local character, e.g. those corresponding to overlaps of type S_6-S_9 (see Table IX). These interactions are larger than those between orbitals located at opposite vertices, which were included in ref 28 but have been neglected here. These additional interactions were necessary for matching the spectrum from the all-electron DV results described above.

(27) Mingos, D. M. P. *J. Chem. Soc., Dalton Trans.* **1974**, 133.
(28) Cotton, F. A.; Haas, T. E. *Inorg. Chem.* **1964**, *3*, 10.

Contribution from the Department of Chemistry,
Miami University, Oxford, Ohio 45056

Kinetics and Mechanism of the Complex Formation of the Chlorite Ion and Iron(III) in Aqueous Solution

István Fábián† and Gilbert Gordon*

Received April 25, 1991

On the basis of rapid-scan spectrophotometric and one-wavelength stopped-flow experiments, the formation of the $FeClO_2^{2+}$ complex was confirmed in the iron(III)-chlorite ion system. The complex formation is associated with the appearance of a new charge-transfer band in the visible spectral region. The stability constant of $FeClO_2^{2+}$ was calculated from the final absorbance value of stopped-flow traces recorded at 510 nm. $\log K = 1.14 \pm 0.02$ and $\epsilon_{510} = 636 \pm 10$ M^{-1} cm^{-1} ($I = 1.0$ M ($NaClO_4$), 25 °C). It was demonstrated that the complex formation is kinetically coupled with catalytic decomposition of ClO_2^-. The proposed mechanism for the ligand substitution reaction includes the reactions of Fe^{3+} and $Fe(OH)^{2+}$ and also a generalized pathway for the chlorite ion decomposition. The rate constant for the $Fe^{3+} + ClO_2^- = FeClO_2^{2+}$ step, 269 ± 55 M^{-1} s^{-1}, is consistent with an associative interchange mechanism predicted by previous kinetic data for complex formation reactions of Fe(III).

Introduction

Oxidation-reduction reactions of chlorite ion have been the subject of extensive kinetic studies in recent years. In the oxidation of metal ions, complex formation with chlorite ion or chlorous acid is generally considered one of the key reaction steps in the detailed mechanisms.[1-3] Although chlorito complexes are of kinetic importance in these systems, the properties of chlorite ion as a ligand are virtually unknown.

The synthesis and redox properties of $Co(NH_3)_5ClO_2^{2+}$ were discussed by Thompson in detail.[4] However, no kinetic or equilibrium data are available for the formation of this inert chlorito complex. Until recently, the only labile metal complex of ClO_2^- was that with the uranyl ion reported by Gordon and Kern.[5] This species was detected in the oxidation of uranium(IV) by chlorine(III), and a rough estimate was given for its stability constant.

Earlier, we reported the formation of $CuClO_2^+$ in aqueous solutions containing Cu^{2+} and ClO_2^-.[6] A relatively weak complex, $CuClO_2^+$ is characterized by an intense absorbance band in the near-UV-visible spectral region ($\lambda_{max} = 387$ nm, $\epsilon_{max} = 1990 \pm 120$ M^{-1} cm^{-1}). It has a stability constant $K = 1.04 \pm 0.07$ M^{-1}, conveniently determined by using stopped-flow-rapid-scan spectrophotometry. This technique was applied in order to avoid spectral interference from the copper(II)-catalyzed decomposition of the chlorite ion. On the basis of these results, the formation of chlorito complexes is expected to be common in any reaction system containing a transition-metal ion and the chlorite ion.

Proper characterization of the coordination chemistry of the chlorite ion requires additional equilibrium and kinetic data for its various complex formation reactions. The iron(III)-ClO_2^- system appears to be one of the best choices for further studies. First of all, +3 is the most stable oxidation state of iron in aqueous solution.[7] Accordingly, no redox reaction between the metal ion and ClO_2^-, which could compete with the complex formation, is expected in this system. Also, Fe^{3+} tends to form more stable complexes than Cu^{2+}.[8] In principle, the complex formation can be monitored by using more preferable experimental conditions, i.e. lower concentration levels, than in the Cu^{2+}-chlorite ion system. The interference from side reactions is presumably decreased by

†On leave from the Institute of Inorganic and Analytical Chemistry, Kossuth L. University, Debrecen, Hungary.

(1) Ondrus, M. G.; Gordon, G. *Inorg. Chem.* **1972**, *11*, 985.
(2) Buchacek, R.; Gordon, G. *Inorg. Chem.* **1972**, *11*, 2154.
(3) Cornelius, R. D.; Gordon, G. *Inorg. Chem.* **1976**, *15*, 1002.
(4) Thompson, R. C. *Inorg. Chem.* **1979**, *18*, 2379.
(5) Gordon, G.; Kern, D. M. H. *Inorg. Chem.* **1964**, *3*, 1055.
(6) Fábián, I.; Gordon, G. *Inorg. Chem.*, in press.
(7) Nelson, S. M. In *Comprehensive Coordination Chemistry*, 1st ed.; Wilkinson, G., Gillard, G., McCleverty, J. A., Eds.; Pergamon: Oxford, U.K., 1987; Vol. 4, pp 217-276 and references therein.
(8) (a) Sillén, L. G.; Martell, A. E. *Stability Constants*; Chemical Society: London, 1964; Suppl. No. 1, 1971. (b) *Stability Constants of Metal-Ion Complexes, Part A: Inorganic Ligands*; IUPAC Chemical Data Series No. 21; Högfeldt, E., Ed.; Pergamon: Oxford, U.K., 1982.

0020-1669/91/1330-3994$02.50/0